OPEN ACCESS
JOURNAL OF ADVANCED DIELECTRICS
Vol. 11, No. 2 (2021) 2150014 (10 pages)

DOI: 10.1142/S2010135X21500144

Influence of sintering behavior on the microstructure and electrical properties of $BaTiO_3$ lead-free ceramics from hydrothermal synthesized precursor nanoparticles

Do Viet On*, Le Dai Vuong†, Truong Van Chuong*, Dao Anh Quang†, Ho Van Tuyen‡,§ and Vo Thanh Tung*,¶

*Department of Physics, College of Sciences
Hue University, Hue City, Vietnam

†Faculty of Chemical and Environmental Engineering
Hue Industrial College, Hue City, Vietnam

‡Institute of Research and Development
Duy Tan University, Da Nang City, Vietnam

§Faculty of Natural Sciences, Duy Tan University
Da Nang City, Vietnam

¶vttung@hueuni.edu.vn

Received 3 March 2021; Revised 31 March 2021; Accepted 5 April 2021; Published 8 May 2021

$BaTiO_3$ nanoparticles were synthesized by hydrothermal method using amorphous phase TiO_2 precursor as the Ti-source. The microstructure and phase structure were determined using XRD, SEM and Raman spectroscopy analysis results. The results showed that $BaTiO_3$ nanoparticles have tetragonal structure, average size of about 100 nm was obtained at Ba/Ti ratio of 1.5, synthesis temperature of 200 °C and reaction time of 12 h. The components of the $BaTiO_3$ lead-free ceramic system are fabricated by conventional solid-phase reaction from the average size $BaTiO_3$ particles about 100 nm obtained by hydrothermal process. The effects of sintering behavior on dielectric, ferroelectric and piezoelectric properties of BT high-density ceramic were studied. The $BaTiO_3$ ceramic composition sintered at 1300 °C has a relative density of 97%, the value of the electromechanical coefficient $k_p = 0.40$, $k_{33} = 0.42$, the large piezoelectric coefficient $d_{33} = 300$ pC/N, $d_{31} = -125$ pC/N.

Keywords: $BaTiO_3$ nanoparticles; lead-free ceramics; piezoelectric; ferroelectric properties.

1. Introduction

Lead zirconate titanate $Pb(Zr_{1-x}Ti_x)O_3$ (PZT)-based piezoelectric ceramics are used in many electronic devices such as ultrasonic generators,[1–3] sensors,[4,5] resonators and actuators,[6,7] memory[8] because of their excellent piezoelectric properties. However, the toxicity of lead in PZT ceramics badly affect the environment and human health.[7,9–11] Therefore, the production of high-performance lead-free piezoelectric ceramics has attracted the attention of many scientists in recent years. Many lead-free ceramic systems are studied as materials based on $Bi_{0.5}Na_{0.5}TiO_3$ (BNT),[12–14] $Bi_{0.5}K_{0.5}TiO_3$ (BKT),[9,15] $BiFeO_3$ (BFO),[16,17] $K_{0.5}Na_{0.5}NbO_3$ (KNN)[18–20] and $BaTiO_3$ (BT).[21–29] Among them, BT-based materials are potential candidates with high piezoelectric properties that can replace PZT.[30,31] Many studies on the BT system to enhance piezoelectric properties are according to different techniques such as microwave sintering, spark plasma sintering, two-step sintering and template grain growth using hydrothermally synthesized fine $BaTiO_3$ powders with high piezoelectric coefficients.[21,25,32,33] Besides, Ma *et al.* made $BaTiO_3$ ceramics by conventional sintering technique from nanopowders. The ceramics sintered at 1190 °C showed the excellent piezoelectrical properties d_{33} = 355 pC/N, which are originated to the contributions of both the crystallographic structure transition and nanodomain.[34] Hu *et al.* reported a high d_{33} value of 420 pC/N for $BaTiO_3$ ceramics fabricated by a facile modified (nanoscale precursors) solid-phase method.[35] These breakthroughs have demonstrated the amazing potential of lead-free materials based on $BaTiO_3$, and showed that the bulk density, microstructures such as pore size, pore morphology and grain size of ceramics directly impacted on the piezoelectric properties of the materials.[23] It can be seen that the nanoparticles used as starting materials and the synthesis technique greatly affect the physical properties of the ceramic. Therefore, different methods are applied for the synthesis of ultrafine powder and high homogeneity such as oxalate,[36] sol–gel,[37] co-precipitation,[38] and hydrothermal process.[39–43] In particular, the hydrothermal process is an

¶Corresponding author.

effective method for the industrial production requirements of $BaTiO_3$ nanopowder due to the attractive processing properties of low-temperature treatment without the need for calcination and grinding.[44]

In this study, we propose a method to fabricate $BaTiO_3$ nanoparticles by hydrothermal method using amorphous TiO_2 nanoparticles fabricated by the ultrasonic-assisted sulfuric acid method and $Ba(OH)_2.8H_2O$ as raw material. The effects of hydrothermal time parameters on the phase transition, morphology and particle size of $BaTiO_3$ nanoparticles were studied. Under optimal conditions, $BaTiO_3$ nanoparticles are used to fabricate high-density bulk ceramics by the conventional solid-phase route. The effects of sintered behavior on the structure, microstructure, dielectric properties, ferroelectric and piezoelectric have been studied in detail.

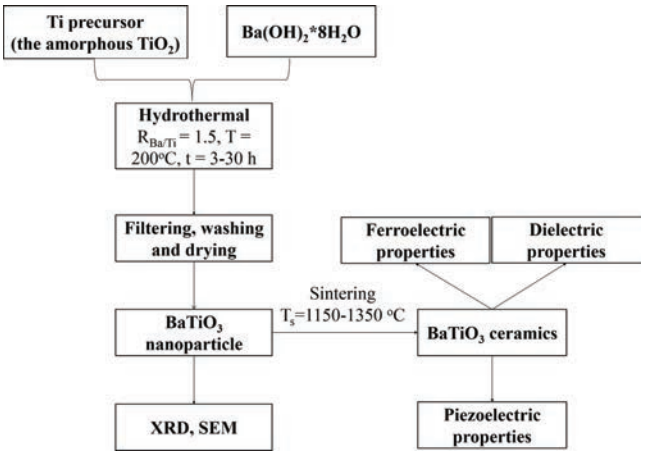

Fig. 1. Flowchart for the preparation of $BaTiO_3$ ceramics.

2. Experimental Procedure

2.1. *Synthesis of $BaTiO_3$ nanoparticles*

$BaTiO_3$ nanoparticles are synthesized using the hydrothermal process according to the following steps. First, amorphous titanium dioxide nanoparticles were synthesized by the sulfuric acid method with the help of ultrasonic waves as in the studies.[45] Titanium dioxide powder (98%, DeaJung-Korea) was dispersed in H_2SO_4 solution using an ultrasonic device (100 W, 28 kHz) for 30 min. Then, the compound is added to distilled water and heated at 100 °C for 2 h. Next, NH_4OH solution is used to adjust the pH of the mixture to a neutral medium. The white precipitate was filtered and washed several times with hot distilled water and then treated at 100 °C for 24 h. The white powders were used as the Ti source during the hydrothermal synthesis of $BaTiO_3$ nanoparticles.

Second, $Ba(OH)_2.8H_2O$ was dissolved in 80 mL of hot distilled water and TiO_2 precursor added to the solution according to the molar ratio of Ba/Ti ($R_{Ba/Ti}$ = 1.5). After 60-min stirring, the mixture was transferred into a Teflon-lined autoclave until 80% of its total volume, and then the autoclave was heated at 200 °C according to different times (t = 3–30 h). After the autoclave was cooled down to room temperature naturally, the white precipitates were collected via centrifugation, washed with hot deionized water and ethanol many times and dried at 100 °C for 24 h. Finally, $BaTiO_3$ powder was finely ground with an agate mortar and used to study properties as shown in the diagram in Fig. 1.

2.2. *Preparation of $BaTiO_3$ ceramics by solid-phase reaction technique*

$BaTiO_3$ nanopowder mixed with 5 wt.% of polyvinyl alcohol (PVA) as a binder to prepare green ceramic discs. The discs were pressed in a hardened stainless-steel die with 12 mm diameter and 1.5 mm in thickness under a load of 150 MPa using a uniaxial press. Then the green pellets were heated at 650 °C for 2 h for binder removal. Finally, $BaTiO_3$ ceramics were sintered by a conventional sintering method at different temperatures (from 1150 °C to 1350 °C, temperature interval for 50 °C) and kept for 4 h.

2.3. *Characterization*

The crystalline structure of the $BaTiO_3$ nanoparticles, and sintered ceramics were analyzed by X-ray diffraction (XRD) analysis (D8-Advanced, BRUKER AXS) at room temperature. The surface morphology was studied using (SEM, JEOL–5300) scanning electron microscopy. Raman scattering spectra were measured using LABRAM-1B (Horiba Jobin-Yvon). The grain size and size distribution of the samples were determined via SEM image analysis performed by using ImageJ. The densities of the samples were measured by the Archimedes method using ethanol. The silver pastes are swept on both sides of the sample and heated at 500 °C for 30 min to create an electrode for electrical measurements. Dielectric properties were obtained by measuring the temperature dependencies of capacitance and phase angle (HIOKI 3532) of the samples in a temperature range of 27–150 °C. To check piezoelectric responses, the specimen was poled in a 100 °C silicone oil bath by applying a DC electric field of 3 kV/mm for 30 min, then cooling to room temperature. The specimens were aged for a day before testing. The electromechanical factors (k) and the piezoelectric strain coefficients (d_{33}, d_{31}) were determined using a resonance method (Agilent 4396B and HIOKI 3532) and calculated the following formulae in the IEEE standard. Ferroelectric properties were determined by Sawyer–Tower circuit method.

3. Results and Discussion

3.1. *Characteristics of $BaTiO_3$ nanopowders*

To get a comprehensive picture of the evolution process, the effect of hydrothermal time on the formation of $BaTiO_3$

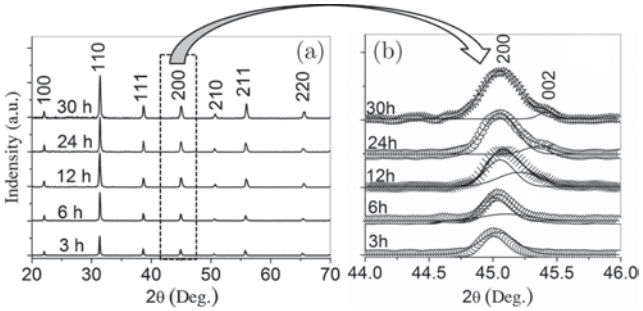

Fig. 2. Typical XRD of $BaTiO_3$ samples synthesized with $R_{Ba/Ti}$ = 1.5 by hydrothermal treatment at 200 °C for various durations (3–30 h).

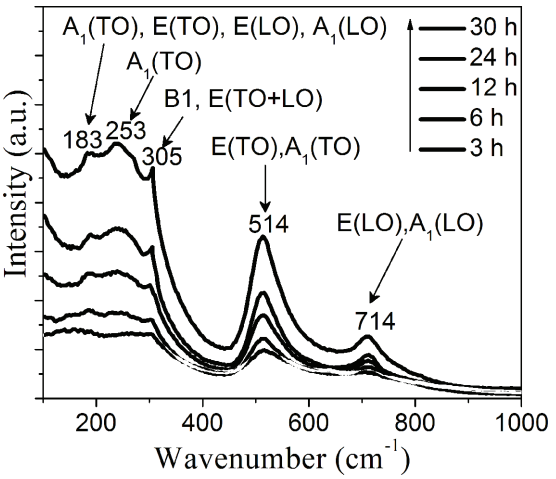

Fig. 3. Raman spectra of the $BaTiO_3$ samples synthesized with $R_{Ba/Ti}$ = 1.5 by hydrothermal treatment at 200 °C for various durations (3–30 h).

nanocrystals (Fig. 2) was studied under the following conditions: $R_{Ba/Ti}$ = 1.5, T = 200 °C and t = 3–30 h.

Figure 2 shows the XRD spectra of the respective samples. Figure 2(a) shows that the diffraction peaks of all samples represent a cubic or tetragonal phase structure. Additionally, the XRD diagram does not contain any other impure phase peaks. As shown in Fig. 2(b), further XRD analysis was performed in the 2θ range from 44° to 46° clearly and revealed a phase transformation from cubic to tetragonal structure with increase in hydrothermal time. The synthesized $BaTiO_3$ nanocrystals were in reaction time 3–6 h, the XRD peaks at angle 2$\theta \approx 45°$ existed single peak corresponding to cubic phase of $BaTiO_3$. However, the hydrothermal time is extended from 12 to 30 h, the XRD peaks at around 45° become wider and tend to split into two peaks corresponding to (200) and (002) of the tetragonal phase as shown in Fig. 2(b). XRD spectroscopy shows that $BaTiO_3$ samples obtained with longer hydrothermal times favor the tetragonal phase formation.[41,42]

Raman spectrum of $BaTiO_3$ samples obtained with hydrothermal time different from 3–30 h is shown in Fig. 3. The bands at 183, 253 and 514 cm^{-1} were observed both in the cubic and tetragonal phases of the $BaTiO_3$ crystal, and can be attributed to scattering from the A_1(TO) phonons.[46,47] The tetragonal phase is confirmed by the relative intensities of the bands at 305 and 714 cm^{-1}, and can be attributed to scattering from phonons B_1 and A_1(LO).[46,47] Moreover, the band at 305 cm^{-1} is related to the E(TO) or B_1 modes, signifying the asymmetry within the [TiO_6] octahedra, while the band at 714 cm^{-1} is emitted from the highest-wavenumber longitudinal optical mode (LO) of A_1 symmetry.[46,47] As shown in Fig. 3, the relative strengths of the bands at 305 and 714 cm^{-1} increase as a function of hydrothermal time, suggesting that an extended hydrothermal time would favor an increase in the amount of tetragonal phase in the $BaTiO_3$ crystal. The Raman results are quite consistent with the peak displacement of the samples in the XRD spectrum (Fig. 2).

Figures 4(a)–4(e) shows SEM image of $BaTiO_3$ samples obtained with different hydrothermal times. The $BaTiO_3$ samples were obtained during a short hydrothermal period of 3 h with a small particle size, which tended to agglomerate to form larger particles and an average size of about 56 nm (Fig. 4(a)). When the hydrothermal time increased to 6 h (Fig. 4(b)), the mean particle size of the sample increased and the agglomeration decreased. For $BaTiO_3$ samples synthesized over a period of 12 h (Fig. 4(c)), the spherical particles have an average size of about 100 nm, copper distribution and good dispersion. When the time was extended from 24 to 30 h (Figs. 4(d) and 4(e)), the mean size of the particles increased and distributed over a wider range. $BaTiO_3$ particle size increased from 56 to 138 nm as the hydrothermal time increased from 3 to 30 h as shown in Fig. 4(f). The efficiency of the $BaTiO_3$ samples was about 80% with a hydrothermal time of 3 h because the reaction was incomplete. When the hydrothermal time increased to 12 h, the yield of the $BaTiO_3$ samples was nearly 93% and decreased slightly with the prolonged synthesis time (Fig. 4(f)). Thus, the spherical BT nanoparticles obtained with the synthesis time of 12 h have an average size of about 100 nm, uniform distribution and high dispersion. These nanoparticles are suitable for fabricating a $BaTiO_3$ lead-free ceramic with good electrical properties as shown in the next section.

3.2. *Effect of sintering temperature on the properties of $BaTiO_3$ ceramic*

$BaTiO_3$ ceramics are fabricated using the conventional sintering method from uniform spherical nanoparticles with an average size of about 100 nm, the nanoparticles were obtained by hydrothermal method under conditions with the Ba/Ti ratio of 1.5, the reaction temperature at 200 °C for 12 h as described in the previous section. The physical properties of $BaTiO_3$ ceramics such as structure, microstructure, dielectric

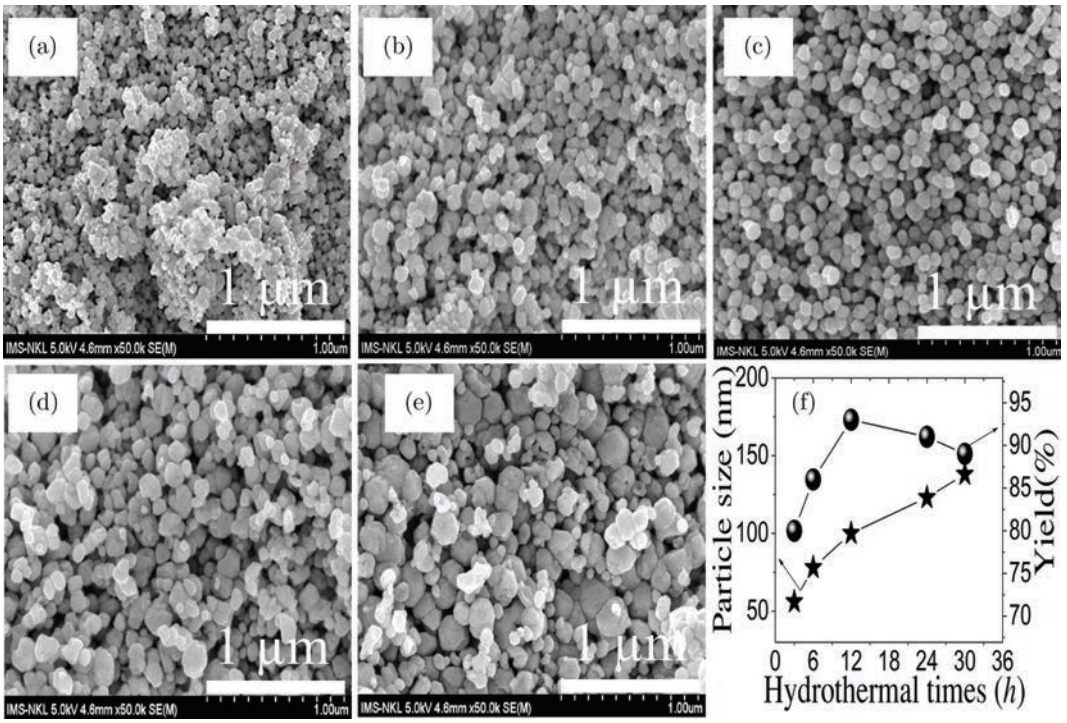

Fig. 4. (a)–(e) SEM images and particle size distribution of $BaTiO_3$ samples obtained with $R_{Ba/Ti} = 1.5$ by hydrothermally treating at temperature 200 °C for various time (t = 3–30 h). (f) A plot of the particle size and yields of the $BaTiO_3$ samples as a function of hydrothermal time.

Table 1. Density, relative density, densification and total shrinkage after sintering of $BaTiO_3$ ceramics as a function of sintering temperature.

Sintered temperatures (°C)	Density (g/cm^3)	Relative density (%)	Densification factor	Shrinkage after sintering (%)
1150	5.20	86.52	0.69	11.67
1200	5.47	91.01	0.83	12.52
1250	5.68	94.51	0.85	12.92
1300	5.83	97.00	0.91	13.44
1350	5.76	95.84	0.88	13.75

properties, and ferro-piezoelectric are strongly dependent on the sintering temperature.[35] Therefore, the effect of the sintering temperature on the physical properties of the ceramic system is studied in this study.

The densification factor (DF) of $BaTiO_3$ ceramics at different sintering temperatures is calculated using Eq. (1):

$$\mathrm{DF} = \frac{\rho_m - \rho_g}{\rho_t - \rho_g}, \tag{1}$$

where ρ_t is the theoretical density, ρ_m is the measured density and ρ_g is the density of green pellets without sintering.[48,49] Shrinkage measurements checked the diameters of both pre-sintered samples using Eq. (2):

$$D_{\text{shrinkage}} = \left(\frac{d_o - d_s}{d_o}\right) \times 100\%, \tag{2}$$

where d_o and d_s are the diameter of the green and sintered pellets, respectively.[48] The densification factor increased with the increase in temperature until it reached the highest contraction, a positive densification factor indicates shrinkage of ceramics at sintering temperatures.[49,50] Table 1 also expresses the shrinkage ratio of the ceramics as a function of sintering temperature. While the shrinkage ratio exhibits an increasing trend of 11.67% to 13.75% up to the sintering temperature of 1300 °C, the ratio decreased slightly above that temperature. The relation between the sintering and shrinkage ratio depends on thermal dilatation.[49,50] The varying trend in the density of the ceramics at different temperatures is similar to the trend of the densification factor. When the sintering temperature increased from 1150 °C to 1350 °C, the density of the samples increased from 5.20 to 5.83 g/cm^3 reaching the highest value of 5.83 g/cm^3 (relative density 97% of the theoretical value and the theoretical density of 6.01 g/cm^3, see Ref. 21) at 1300 °C, upon which it then decreased.

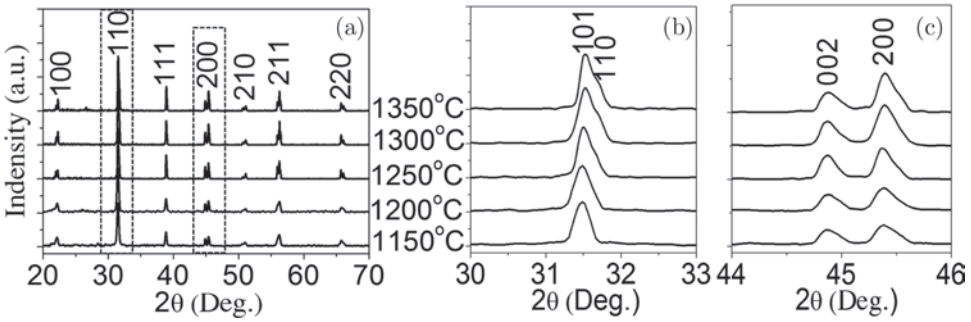

Fig. 5. XRD patterns of the $BaTiO_3$ ceramics with different sintering temperatures corresponding to 2θ from (a) 20–70°, (b) 30–33° and (c) 44–46°.

Figure 5 shows the XRD patterns of poled $BaTiO_3$ ceramics sintered at different temperatures from 1150 °C to 1350 °C. All the samples have a pure perovskite structure without any trace of impurity phase (Fig. 5(a)). X-ray diffraction spectra in the range close to 31.5° showed peak (101) having a single peak at 1150 °C and 1200 °C. When the sintering temperature increases, the diffraction peak with 2θ around 31.5° tends to expand towards a large angle and splits into two peaks (101) and (110) respectively as shown in Fig. 5(b). Figure 5(c) shows an extended XRD spectrum in the range 45° at sintering temperatures between 1150 °C and −1350 °C, the two diffraction peaks respectively (002) and (200) are characteristic of the tetragonal phase structure of $BaTiO_3$ material. The intensity of two diffraction peaks $I_{(002)}$ and $I_{(200)}$ has a change with the sintering temperature. The peak intensity increases as the heating temperature increases from 1150 °C to 1300 °C and then decreases. The decreased diffraction 2θ peak corresponds to the enlargement of the lattices. There may be some oxygen vacancies in lattice due to inadequate oxygen supply in the environment with raising sintering temperature, leading to the substitution of Ti^{3+} (0.72 Å) for Ti^{4+} (0.68 Å) results in the enlargement of lattice.[34,51,52]

Figure 6 shows the variation in the lattice parameters (a, c) and tetragonality (c/a) of the $BaTiO_3$ ceramics with different sintering temperatures. The sample sintered at 1150 °C shows a tetragonal symmetry, whose lattice parameters are $a = b =$ 3.9840 Å and c = 4.0094 Å. With increasing temperature, constant a increases and c decreases slightly, whereas tetragonality (c/a) increases as sintering temperature increases and reaches the maximum value (1.0075) at 1300 °C. The change in the lattice parameters is consistent with the change in intensity of X-ray diffraction as shown in Fig. 5.

Figure 7 shows the SEM image of the $BaTiO_3$ ceramic system according to different sintering temperatures. The $BaTiO_3$ ceramic sintered at 1150 °C shows a loose structure, the particles are discrete bound, resulting in low ceramic density. When the temperature increases at 1200 °C, the particles begin to bond together, however, the pore density is quite large. At the heating temperature of 1250 °C, the particles

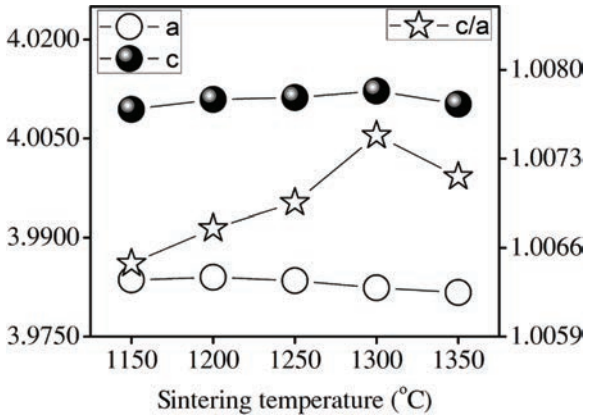

Fig. 6. Lattice parameters and tetragonality for the $BaTiO_3$ ceramics with different sintering temperatures.

grew bound together, and no voids were observed. However, the surface microstructure and the boundaries between the particles are not clear. The sintering temperature increases to 1300 °C, the pore almost disappears, the grain boundary is tightly bound to create a high-density ceramic. Continuing to increase the temperature to 1350 °C, grain size develops, pores appear at the border and in the seed. The sintered samples at 1300 °C reach the maximum density 97.00% and grain value of 3.18 μm.

Figure 8(a) shows the dependence of the electromechanical coupling coefficient k by sintering temperature. All coefficients k_p, k_{31} and k_{33} have the same rules, increasing when the temperature increases from 1150 °C to 1300 °C and reaches the maximum values of 0.40, 0.22 and 0.43. The temperature continued to increase to 1350 °C, the coefficients were reduced as in Table 2. The piezoelectric coefficients d_{31} and d_{33} of $BaTiO_3$ ceramics depend on the sintering temperature as shown in Fig. 8(b). The piezoelectric properties rapidly increase with the heat reaching the maximum value at 1300 °C and decreasing as the temperature increases. This rule is similar to the sintered temperature dependence of density and particle size, indicating that density and particle size are important factors contributing to

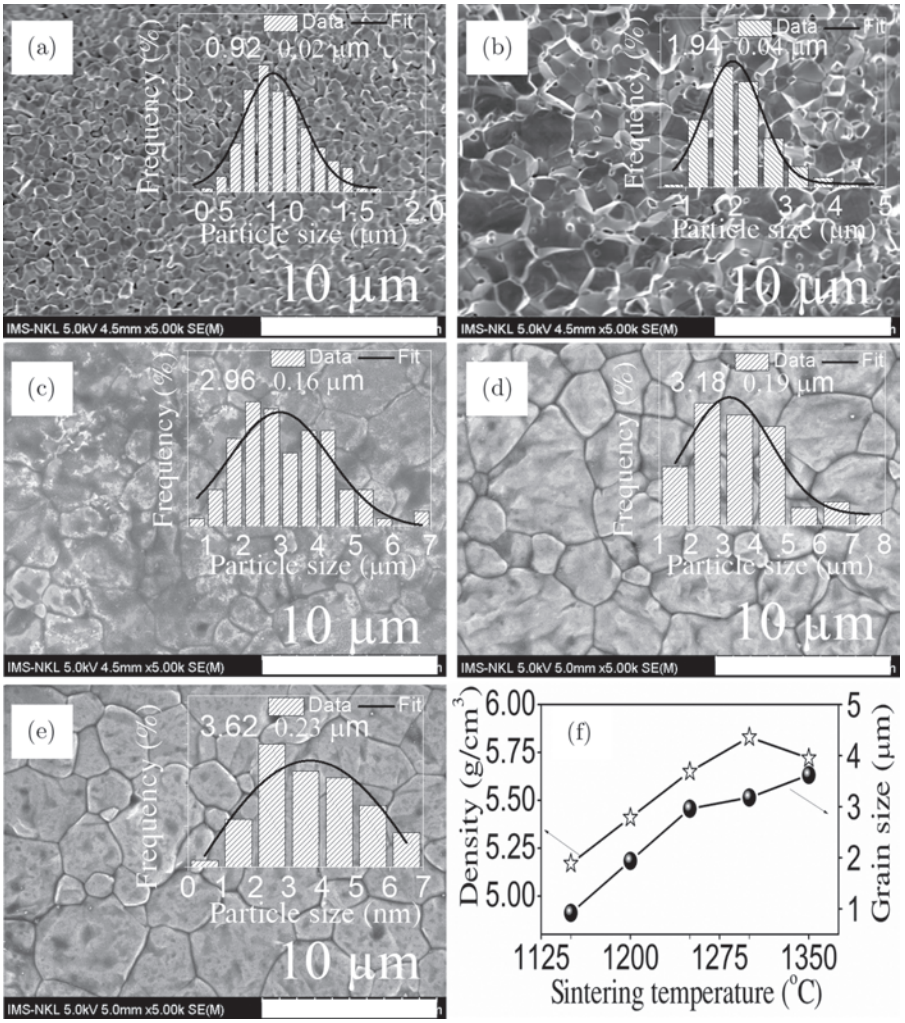

Fig. 7. (a)–(e) SEM images of the $BaTiO_3$ ceramics sintered at different temperatures. (f) Density and particle size of $BaTiO_3$ ceramics as functions of the sintering temperature.

the high piezoelectric effect in sintered $BaTiO_3$ ceramics at 1300 °C (set as Table 2).[34] It is known that oxygen vacancies are major structural defects in the barium titanate generated due to loss of oxygen during sintering at high temperature in accordance with following relation, a process defined by Kronger–Vink notation.[52]

$$V_o \rightarrow \frac{1}{2}O_2 + V_0'' + 2e. \quad (3)$$

Electrons created by ionization of thermally activated oxygen vacancies captured by Ti^{4+} cause the hopping of electrons between Ti^{4+} and Ti^{3+} that may attribute to the enhanced electric response in the studied ceramics (Fig. 8).[52] In addition, the piezoelectric properties of the ceramic system are related to the varying intensity ratio of diffraction peaks (002) and (200). When the temperature increases from 1150 °C to 1350°C, the intensity ratio of the two peaks increases corresponding to the phase ratio of the tetragonal increase and reaches its maximum value at 1300 °C. Therefore, the electrical properties of ceramics at this temperature are best and then gradually decrease as shown in Fig. 8.

Figure 9 shows the dielectric constant dependence according to the temperature measured at 10 kHz of the sintered $BaTiO_3$ ceramic system at different temperatures. The ε_r–T curves of all the samples exhibited one sharp peak, which was corresponding to the ferroelectric tetragonal–paraelectric cubic phase transition at the Curie temperature (T_c).[34] Curie temperature changed in the range of 123–125 °C and reached the maximum value of 125 °C at the sintered temperature of 1350 °C. The samples sintered at 1300 °C shows the highest dielectric constant at Curie temperature T_C. According to Ma, oxygen drum positions can consume energy and damage dielectric properties. Improved density reduction results reduce the oxygen drum position, so the dielectric constant is increased.[34]

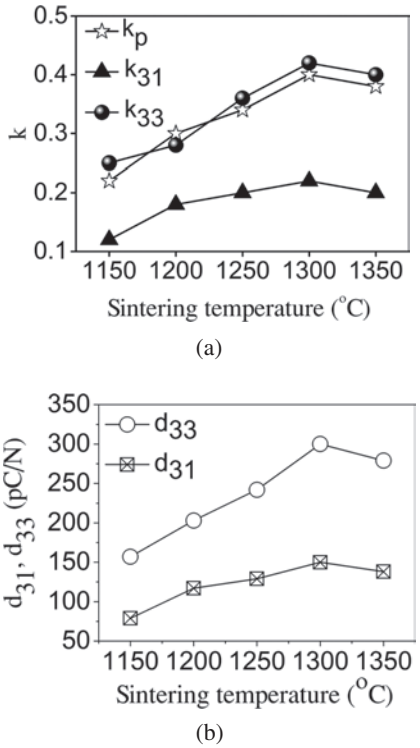

Fig. 8. (a) Electromechanical coefficient k and (b) piezoelectric constant d, g of the $BaTiO_3$ ceramics as functions of the sintering temperature.

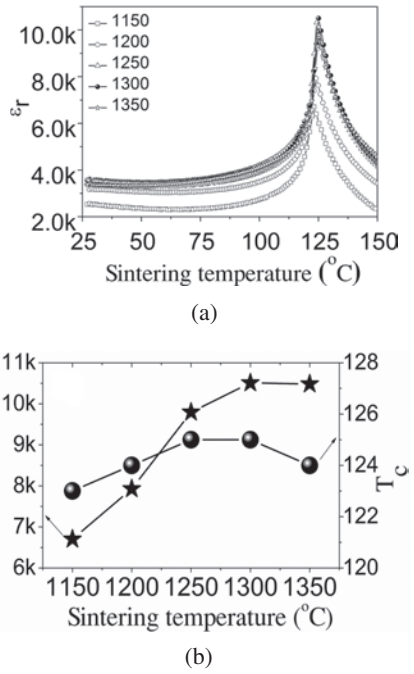

Fig. 9. Temperature dependence of the dielectric constant and Curie temperature for the temperature of the $BaTiO_3$ ceramics sintered at 1150–1350 °C.

Table 2. Physical properties of $BaTiO_3$ ceramics at room temperature.

	Sintering temperature				
	1150 °C	1200 °C	1250 °C	1300 °C	1350 °C
ρ (g·cm^{-3})	5.20	5.47	5.68	5.83	5.76
ε' at 1 kHz	2612	3226	3405	3587	3436
T_C (°C)	123	124	125	125	124
Tan δ	0.05	0.04	0.03	0.03	0.04
d_{33} (pC/N)	147	203	242	300	279
d_{31} (pC/N)	−79	−117	−129	−150	138
k_p	0.22	0.30	0.34	0.40	0.38
k_{33}	0.25	0.28	0.36	0.42	0.40
k_{31}	0.12	0.18	0.20	0.22	0.20

Figure 10(a) shows the ferroelectric hysteresis loops of the ceramics sintered at different temperature values. All samples had a polarization hysteresis loop of typical ferroelectric materials. The remnant polarization P_r and coercive

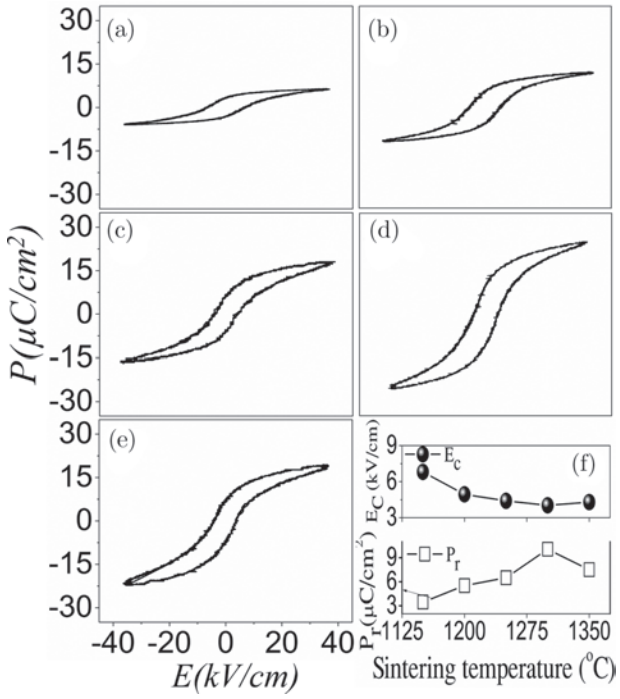

Fig. 10. Ferroelectric hysteresis loops (P–E) of the $BaTiO_3$ ceramics with different temperatures and (b) evolutions of P_r and E_c as functions of sintering temperature.

Table 3. The comparison of the characteristic parameters of the $BaTiO_3$ ceramics and other ceramics.

Ceramics	Size of the original material	T_S (°C)	k_p	d_{33} (pC/N)	T_C (°C)	E_c (kV/cm)	P_r (μm/cm^2)	Refs.
$BaTiO_3$	micro	>1350	—	190	120	—	—	53
$BaTiO_3$	nano	1300	—	240	120	3.54	11.78	35
$BaTiO_3$–4%mol LiF	nano	1100	0.45	270	73	3.89	9.5	24
BaTiO–0.05%mol Li_2O	nano	1050	—	200	120	8.0	2.0	22
$BaTiO_3$–3at.% Li_2CO_3	nano	1300	0.43	260	130	—	—	54
$BaTiO_3$	nano	1300	0.40	300	125	4.03	10.06	This work

field E_C for $BaTiO_3$ ceramic sintered at different temperatures are described in Fig. 10(b). The first P_r increases from 3.29 to 10.06 μC/cm^2 (1300 °C) and then decreases to 6.85 μC/cm^2 (1350 °C), while the E_C decreases from 6.75 to 4.13 kV/cm (1300 °C) and finally increases to 4.54 kV/cm (1350 °C). Samples sintered at 1300 °C have a maximum P_r value of 10.06 μC/cm^2 with a corresponding E_C value of 4.13 kV/cm, indicating that this ceramic is more easily polarized and has higher piezoelectricity. However, oxygen drum positions are easier to create at higher sintering temperatures, resulting in an obstruction effect of the ferroelectric domain under an electric field, thereby creating an increase of E_C and depletion of P_r.[34]

To confirm the achievements of this study, the characteristic parameters of the sample $BaTiO_3$ sintered at 1300 °C such as the sintering temperature (*Ts*), electromechanical coupling coefficient (k_p), piezoelectric coefficients (d_{33}), Curie temperature (T_C), the remnant polarization (P_r) and coercive field (E_C) were extracted and compared with those of other $BaTiO_3$-based lead-free ceramics[22,24,35,53,54] as listed in Table 3. Our results indicate that $BaTiO_3$ ceramics with nano-sized starting materials have lower sintering temperatures than micro-sized, while the electrical properties of ceramic materials are well maintained.

4. Conclusion

The following results were concluded in this study: $BaTiO_3$ spherical nanoparticles are distributed uniformly with average size of about 100 nm obtained by hydrothermal process with optimal parameters corresponding to a Ba/Ti ratio of 1.5, the reaction temperature at 200 °C during time duration of 12 h. $BaTiO_3$ piezoelectric ceramics were successfully fabricated from hydrothermal powders by the conventional solid-state reaction. Excellent piezoelectric properties were found in sintered samples at 1300 °C expressed in parameters d_{33} = 300 pC/N, d_{31} = −125 pC/N, k_p = 0.40 and k_{33} = 0.42. The relative density value is 97.00% compared with the theoretical density and the particle size of 3.18 μm contributes to the high piezoelectric properties in $BaTiO_3$ ceramics.

Acknowledgment

This work was carried out in the framework of the National Project in Physics Program until 2020 under No. ĐTĐLCN.10/18 (PI: Associate Professor Vo Thanh Tung from University of Sciences, Hue University).

References

[1]L. D. Vuong, P. D. Gio, N. D. V. Quang, T. D. Hieu and T. P. Nam, Development of $0.8Pb(Zr_{0.48}Ti_{0.52})O_3$–$0.2Pb[(Zn_{1/3}Nb_{2/3})_{0.625}(Mn_{1/3}Nb_{2/3})_{0.375}]O_3$ ceramics for high-intensity ultrasound applications, *J. Electron. Mater.* **47**(10), 5944 (2018).
[2]L. D. Vuong, V. T. Tung and P. D. Gio, The investigation on the fabrication and characterization of the multicomponent ceramics based on PZT and the relaxor PZN-PMnN ferroelectric materials, *Ceramic Materials* (IntechOpen, 2020).
[3]N. D. T. Luan, L. D. Vuong, T. V. Chuong and N. T. Tho, Structure and physical properties of PZT-PMnN-PSN ceramics near the morphological phase boundary, *Adv. Mater. Sci. Eng.* **2014**(5), 1 (2014).
[4]V. Rathod, A review of acoustic impedance matching techniques for piezoelectric sensors and transducers, *Sensors* **20**(14), 4051 (2020).
[5]D. Wang and J. S. Chen, Progress on the applications of piezoelectric materials in sensors, *Mater. Sci. Forum* **848**, 749 (2016).
[6]H. Kabra, H. Deore and P. Patil, Review on advanced piezoelectric materials ($BaTiO_3$, PZT), *J. Emerg. Technol. Innov. Res.* **6**(4), 950 (2019).
[7]E. Aksel and J. Jones, Advances in lead-free piezoelectric materials for sensors and actuators, *Sensors (Basel, Switzerland)* **10**(3), 1935 (2010).
[8]A. Jain, P. J. A. Sharma, A. Jain and R. P.N, Dielectric and piezoelectric properties of PVDF/PZT composites: A review, *Polym. Eng. Sci.* **55**(7), 1589 (2015).
[9]L. D. Vuong and P. D. Gio, Enhancement in dielectric, ferroelectric, and piezoelectric properties of $BaTiO_3$-modified $Bi_{0.5}(Na_{0.4}K_{0.1})TiO_3$ lead-free ceramics, *J. Alloys Compd.* **817**, 152790 (2020).
[10]D. A. Tuan, V. T. Tung, L. D. Vuong, N. H. Yen and L. T. U. Tu, Investigation of phase formation and poling conditions of lead-free $0.48Ba(Zr_{0.2}Ti_{0.8})O_3$-$0.52(Ba_{0.7}Ca_{0.3})TiO_3$ ceramic, **47**(2), 6297 (2018).
[11]D. A. Tuan, L. D. Vuong, V. T. Tung, N. N. Tuan and N. T. Duong, Dielectric and ferroelectric characteristics of doped BZT-BCT ceramics sintered at low temperature, *J. Ceram. Process. Res.* **19**(1), 32 (2018).
[12]C. S. Mallam and P. Kumar, Synthesis and characterizations of BNT–BT and BNT–BT–KNN ceramics for actuator and energy storage applications, *Ceram. Int.* **41**(4), 5574 (2015).

[13]T. Badapanda, S. Sahoo and P. Nayak, Dielectric, ferroelectric and piezoelectric study of BNT-BT solid solutions around the MPB region, *IOP Conf. Series: Mater. Sci. Eng.* **178**(1), 012032 (2017).
[14]G. Song, Z. Liu, F. Zhang, F. Liu, Y. Gu, Z. Liu and Y. Li, High-throughput synthesis and electrical properties of BNT–BT–KNN lead-free piezoelectric ceramics, *J. Mater. Chem. C* **8**(11), 3655 (2020).
[15]D. Hu, Z. Pan, X. Zhang, H. Ye, Z. He, M. Wang, S. Xing, J. Zhai, Q. Fu and J. Liu, Greatly enhanced discharge energy density and efficiency of novel relaxation ferroelectric BNT–BKT-based ceramics, *J. Mater. Chem. C* **8**(2), 591 (2020).
[16]L.-F. Zhu, B.-P. Zhang, Z.-C. Zhang, L.-J. Wang and L.-J. Zheng, Piezoelectric, ferroelectric and ferromagnetic properties of $(1-x)BiFeO_3$–$xBaTiO_3$ lead-free ceramics near morphotropic phase boundary, *J. Mater. Sci.: Mater. Electron.* **29**(3), 2307 (2018).
[17]W. Gao, L. Jing and X. Lou, Large electric-field-induced strain and enhanced piezoelectric constant in CuO modified $BiFeO_3$-$BaTiO_3$ ceramics, *J. Am. Ceram. Soc.* **10**(8), 3383 (2018).
[18]E. Politova, N. Golubko, G. Kaleva, A. Mosunov, N. Sadovskaya, S. Stefanovich, D. Kiselev, A. Kislyuk, M. Chichkov and P. Panda, Structure, ferroelectric and piezoelectric properties of KNN-based perovskite ceramics, *Ferroelectrics* **538**, 45 (2019).
[19]Z. Cen, Y. Huan, W. Feng, Y. Yu, P. Zhao, L. Chen, C. Zhu, L. Li and X. Wang, A high temperature stable piezoelectric strain of KNN-based ceramics, *J. Mater. Chem. A* **6**(41), 19967 (2018).
[20]C. Wang, B. Fang, Y. Qu, Z. Chen, S. Zhang and J. Ding, Preparation of KNN based lead-free piezoelectric ceramics via composition designing and two-step sintering, *J. Alloys Compd.* **832**, 153043 (2019).
[21]Z.-Y. Shen and J. Li, Enhancement of piezoelectric constant d_{33} in $BaTiO_3$ ceramics due to nano-domain structure, *J. Ceram. Soc. Jpn.* **118**, 940 (2010).
[22]N. Ma, Z. B.-P. Zhang and W.-G. Yang, Low-temperature sintering of Li_2O-doped $BaTiO_3$ lead-free piezoelectric ceramics, *J. Electroceram.* **28**, 275 (2012).
[23]J. C. Wang, P. Zheng, R. Q. Yin, L. Zheng, J. Du, L. Zheng, J. Deng, K. Song and H. B. Qin, Different piezoelectric grain size effects in $BaTiO_3$ ceramics, *Ceram. Int.* **41**(10), 14165 (2015).
[24]W.-G. Yang, Z. B.-P. Zhang, N. Ma and L. Zhao, High piezoelectric properties of $BaTiO_3$–XLiF ceramics sintered at low temperatures, *Journal of the European Ceramic Society,* **32**, 899 (2012).
[25]Y. Huan, X. Wang, J. Fang and L. Li, Grain size effect on piezoelectric and ferroelectric properties of $BaTiO_3$ ceramics, *J. Eur. Ceram. Soc.* **34**, 1445 (2014).
[26]W.-B. Li, D. Zhou, W.-F. Liu, J.-Z. Su, F. Hussain, D.-W. Wang, G. Wang, Z.-L. Lu and Q.-P. Wang, High-temperature $BaTiO_3$-based ternary dielectric multilayers for energy storage applications with extreme high efficiency, *Chem. Eng. J.* **414**(28), 128760 (2021).
[27]D. Wang, Z. Fan, G. Rao, G. Wang, Y. Liu, C. Yuan, T. Ma, D. Li, X. Tan, Z. Lu, A. Feteira, S.-Y. Liu, C. Zhou and S. Zhang, Ultrahigh piezoelectricity in lead-free piezoceramics by synergistic design, *Nano Energy* **76**, 104944 (2020).
[28]H. Yang, Z. Lu, L. Li, W. Bao, H. Ji, J. Li, A. Feteira, F. Xu, Y. Zhang, H. Sun, Z. Huang, W. Lou, K. Song, S. Sun, G. Wang, D. Wang and I. M. Reaney, Novel $BaTiO_3$-based, Ag/Pd-compatible lead-free relaxors with superior energy storage performance, *ACS Appl. Mater. Interf.* **12**(39), 43942 (2020).
[29]G. Liu, Y. Li, B. Guo, M. Tang, Q. Li, J. Dong, L. Yu, K. Yu, Y. Yan, D. Wang, L. Zhang, H. Zhang, Z. He and L. Jin, Ultrahigh dielectric breakdown strength and excellent energy storage performance in lead-free barium titanate-based relaxor ferroelectric ceramics via a combined strategy of composition modification, viscous polymer processing, and liquid-phase sintering, *Chem. Eng. J.* **398**, 125625 (2020).
[30]A. Bell, Ferroelectrics: The role of ceramic science and engineering, *J. Eur. Ceram. Soc.* **28**, 1307 (2008).
[31]M. Acosta, N. Novak, V. Rojas, S. Patel, R. Vaish, J. Koruza, G. A. Rossetti Jr. and J. Rödel, $BaTiO_3$-based piezoelectrics: Fundamentals, current status, and perspectives, *Appl. Phys. Rev.* **4**, 041305 (2017).
[32]Y. Huan, X. Wang, J. Fang, L. Li and I. W. Chen, Grain size effects on piezoelectric properties and domain structure of $BaTiO_3$ ceramics prepared by two-step sintering, *J. Am. Ceram. Soc.* **96**(11), 3369 (2013).
[33]S. Wada, K. Takeda, T. Tsurumi and T. Kimura, Preparation of [110] grain oriented barium titanate ceramics by templated grain growth method and their piezoelectric properties, *Int. Symp. Micro-NanoMechatronics and Human Science* (IEEE, Nagoya, Japan, 2007), pp. 372–376.
[34]N. Ma, Z. B.-P. Zhang, W.-G. Yang and D. Guo, Phase structure and nano-domain in high performance of $BaTiO_3$ piezoelectric ceramics, *J. Eur. Ceram. Soc.* **32**, 1059 (2012).
[35]S. Hu, C. Luo, P. Li, J. Hu, G. Li, H. Jiang and W. Zhang, Effect of sintered temperature on structural and piezoelectric properties of barium titanate ceramic prepared by nano-scale precursors, *J. Mater. Sci.: Mater. Electron.* **28**(13), 9322 (2017).
[36]W.-S. Jung, J. Park, Y. Park and D.-H. Yoon, Effects of impurities on the properties of $BaTiO_3$ synthesized from barium titanyl oxalate, *Ceram. Int.* **36**, 1997 (2010).
[37]M.d. A. Gomes, L. G. Magalhães, A. R. Paschoal, Z. S. Macedo, Á. S. Lima, K. I. B. Eguiluz and G. R. Salazar-Banda, An eco-friendly method of $BaTiO_3$ nanoparticle synthesis using coconut water, *J. Nanomater.* **2018**, 5167182 (2018).
[38]A. Sobha and R. Sumangala, Influence of synthesis method and the precursor on the preparationof barium titanate nano particles, *Res. Rev.: J. Mater. Sci.* **6**(3), 175 (2018).
[39]H.-W. Lee, S. Moon, C. H. Choi and D. K. Kim, Synthesis and size control of tetragonal barium titanate nanopowders by facile solvothermal method, *J. Am. Ceram. Soc.* **95**, 2429 (2012).
[40]S. Moon, H.-W. Lee, C. H. Choi and D. K. Kim, Influence of ammonia on properties of nanocrystalline barium titanate particles prepared by a hydrothermal method, *J. Am. Ceram. Soc.* **95**(7), 2248 (2012).
[41]J.-M. Han, M.-R. Joung, J.-S. Kim, Y.-S. Lee, S. Nahm, C. Youn Kyu and J.-H. Paik, Hydrothermal synthesis of $BaTiO_3$ nanopowders using TiO_2 nanoparticles, *J. Am. Ceram. Soc.* **97**(2), 346 (2013).
[42]J. Gao, H. Shi, H. Dong, R. Zhang and D. Chen, Factors influencing formation of highly dispersed BaTiO3 nanospheres with uniform sizes in static hydrothermal synthesis, *J. Nanopart. Res.* **17**(7), 286 (2015).
[43]N. Liu, W. Zhao and J. Rong, CO_2-driven synthesis of monodisperse barium titanate microspheres, *J. Am. Ceram. Soc.* **101**(4), 1407 (2018).
[44]B. W. Lee and S.-B. Cho, Hydrothermal preparation and characterization of ultra-fine $BaTiO_3$ powders from amorphous peroxo-hydroxide precursor, *J. Electroceram.* **13**(1), 379 (2004).
[45]N. T. Duong, L. D. Vuong, N. M. Son, H. V. Tuyen and T. V. Chuong, The synthesis of TiO_2 nanoparticles using sulfuric acid method with the aid of ultrasound, *Nanomater. Energy* **6**, 1 (2017).
[46]Z. Deng, Y. Dai, W. Chen, X. Pei and J. Liao, Synthesis and characterization of bowl-like single-crystalline $BaTiO_3$ nanoparticles, *Nanoscale Res. Lett.* **5**, 1217 (2010).
[47]J. Gao, H. Shi, J. Yang, T. Li, R. Zhang and D. Chen, Influencing factor investigation on dynamic hydrothermal growth of gapped hollow BaTiO3 nanospheres, *Nanoscale Res. Lett.* **10**, 1033 (2015).
[48]M. Alkathy, A. Hezam, K. S. D. Manoja, J. Wang, C. Cheng, K. Byrappa and J. Raju, Effect of sintering temperature on structural, electrical, and ferroelectric properties of lanthanum and sodium co-substituted barium titanate ceramics, *J. Alloys Compd.* **762**, 49 (2018).

[49]N. T. Tho and L. D. Vuong, Sintering behavior and enhanced energy storage performance of SnO_2-modified $Bi_{0.5}(Na_{0.8}K_{0.2})_{0.5}TiO_3$ lead-free ceramics, *J. Electroceram.* 1 (2020).

[50]N. Hana, A. Megriche and M. El Maaoui, Effect of sintering temperature on microstructure and electrical properties of $Sr_{1-x}(Na_{0.5}Bi_{0.5})_xBi_2Nb_2O_9$ solid solutions, *J. Adv. Ceram.* **3**, 17 (2014).

[51]M. Prades, N. Masó, H. Beltrán, E. Cordoncillo and A. R. West, Polymorphism of $BaTiO_3$ acceptor doped with Mn^{3+}, Fe^{3+}, and Ti^{3+}, *J. Am. Ceram. Soc.* **91**(7), 2364 (2008).

[52]N. Sareecha, W. A. Shah, M. Anis-ur-Rehman, M. Mirza and M. S. Awan, Electrical investigations of $BaTiO_3$ ceramics with Ba/Ti contents under influence of temperature, *Solid State Ionics* **303**, 16 (2017).

[53]M. M. Vijatović Petrović, J. D. Bobić and B. Stojanović, History and challenges of barium titanate: Part II, *Sci. Sinter.* **40**, 235 (2008).

[54]T. Kimura, Q. Dong, S. Yin, T. Hashimoto, A. Sasaki, S. Aisawa and T. Sato, Synthesis and piezoelectric properties of Li, Ca and Mn-codoped $BaTiO_3$ by a solvothermal approach, *IOP Conf. Series: Mater. Sci. Eng.* **47**, 012018 (2013).